Springer

KSME

Journal of Mechanical Science and Technology 30 (8) (2016) 3835~3845
www.springerlink.com/content/1738-494x(Print)/1976-3824(Online)
DOI 10.1007/s12206-016-0747-8

Comparative study of MPC and LQC with disturbance rejection control for heavy vehicle rollover prevention in an inclement environment †

Fitri Yakub[1,2,*] Shihao Lee[3] and Yasuchika Mori[2]

[1]*Malaysia-Japan International Institute of Technology, Universiti Teknologi Malaysia, Jln Semarak, 54100, Kuala Lumpur, Malaysia*
[2]*Graduate School of System Design, Tokyo Metropolitan University, Hino, 191-0065, Tokyo, Japan*
[3]*Hitachi LTD, Hitachi, 317-8601, Ibaraki, Japan*

(Manuscript Received February 8, 2015; Revised July 5, 2015; Accepted April 11, 2016)

Abstract

This paper compares the Model predictive control (MPC) and Linear quadratic control (LQC) of heavy vehicles via active front steering for rollover prevention in inclement environments. In both control methods, a Disturbance rejection control (DRC) that negates the effects of wind and road bank acting on the vehicle is designed. Load transfer ratio (LTR) is applied to judge rollover by mitigating the absolute value of LTR as much as possible. We tested and compared two different controllers, i) MPC with DRC and ii) LQC with DRC. Two types of environmental conditions were considered, i) typhoon and ii) typhoon on a bumpy road. The simulation results demonstrate that MPC was more successfully implemented than LQC during LTR suppression. This paper also proposes an MPC for coordination of active rear steering and differential braking control maneuvers to prevent rollover in inclement environments. For a feasible comparison, the LQC controller was designed using the same approach adopted for the MPC controller. Results show the proposed coordinated control yields better performance for rollover prevention than LQC.

Keywords: Heavy vehicle; Model predictive control; Linear quadratic control; Rollover prevention; Disturbance observer; Disturbance rejection control

1. Introduction

Inclement environmental conditions are an important factor in fatal rollovers. A strong lateral wind or significant road bank may harass heavy vehicle behavior, and even initiate rollover accidents, because roll stability is easily affected by these disturbances. Developing a control system for disturbance detection and rollover prevention is important for vehicles moving on an uneven surface or through strong lateral winds.

The disturbance observer (DOB) is an effective compensation mechanism that reduces the effects of disturbances, uncertainties, and nonlinearities within the plant, and enforces nominal input/output behavior, particularly in the low frequency range, where the reference signal frequency is concentrated. Accordingly, the DOB has the ability to reject high-order and stepwise disturbances asymptotically.

In the past few years, the force of wind and moment acting on a vehicle body have been regarded as an unmeasured disturbance that can be estimated and suppressed without changing the input-output behavior by a DOB [1]. Its application to compensate for electric power steering is used to revise yaw rate performance [2]. In Ref. [3], low-order DOB was proven to successfully reduce the computational cost of implementation. The road bank angle can also be precisely estimated using a DOB from a Global positioning system (GPS) and inertial navigation system [4], or from low-cost onboard sensors [5]. Moreover, Ref. [6] presented road bank estimation using a dynamic simplex method for rollover prediction.

Model predictive control (MPC) and Linear quadratic control (LQC), which are based on a quadratic cost function, are widely implemented for process control [7], motion control [8] and vehicle control [9]. The main advantage of LQC is that optimal input signal can be obtained from full state feedback, whereas MPC is optimal when implemented in closed-loop systems. However, LQC has limitations in systems affected by actuator limitations. For instance, restricting the manipulated variable or the controlled variable can be difficult [10].

However, because by design, MPC does not directly handle disturbances, it cannot satisfactorily achieve control vehicle stability in the presence of strong disturbances and large uncertainties. Therefore, DOB with Disturbance rejection control (DRC) acts as an observer and compensator, thereby improving vehicle performance. DOB-MPC-based approaches for

*Corresponding author. Tel.: +60 11 5221 4962, Fax.: +60 3 2203 1266
E-mail address: mfitri.kl@utm.my
† Recommended by Associate Editor Deok Jin Lee

improving tracking performance in the control system have been proposed [11, 12]. However, actual applications in rollover prevention have been rarely demonstrated, and comparisons are rarely made.

In this paper, a DOB and MPC based on DRC are proposed for rollover prevention control, particularly for heavy duty vehicle systems. Unlike conventional DOB, which is only suitable for a minimum-phase system with (or without) time delay, enhanced DOB with DRC can handle a disturbance observer for the non-minimum-phase delay systems in a single lane change scenario. Several simulations are performed to demonstrate the effectiveness of the proposed method, and a comparison is made with the standard LQC and DOB with DRC. This comparison is the main innovation of this paper. To the best of the author's knowledge, previous work has not provided such a comparison for rollover prevention control of heavy vehicles.

The first study focuses on the comparative investigation of MPC and LQC with DRC for autonomous control without driver intervention, in which Active front steering (AFS) is demonstrated for rollover prevention. Several AFS implementations have been conducted [13, 14], with different objectives and scenarios. Here, MPC and LQC are designed with DOB to estimate and suppress the effects of unmeasured disturbances, uncertainties, and nonlinearities. In the DRC design, estimated wind and road bank are used as cancellation signals to provide steering assistance to the driver.

The comparison of the MPC and LQC controllers for rollover prevention and roll damping is our main focus; keeping occupants safe is the top priority in worst-case environmental conditions. The autonomous steering control of a heavy vehicle travelling in a straight line is simulated in two different environmental conditions: Step wind of a typhoon and the combination of the sinusoidal typhoon wind with a random road bank angle.

For the second contribution, we enhance MPC to coordinate Active rear steering (ARS) and Differential braking control (DBC) maneuvers for rollover prevention in the thread avoidance scenario, under the influence of an inclement environment. Differential braking controls have been used in numerous vehicle applications with various control methods and objectives [15, 16]. The front steering angle is assumed to be a disturbance in cases of the driver losing control or in abrupt maneuver scenarios. We propose a braking control algorithm based on the left and right rear wheels rather than on the front and rear wheels.

This paper is structured as follows. An improved vehicle model, tire model, wind force model, and the rollover indicator are introduced in Sec. 2. The structures of the MPC and LQC controllers, including DOB and DRC, are presented in Sec. 3. Control methods for the linear MPC algorithm and rear braking control concept are explained in Sec. 3. Simulation results are analyzed in Sec. 4. Finally, in Sec. 5, some highlights and recommendations for future work are pointed out.

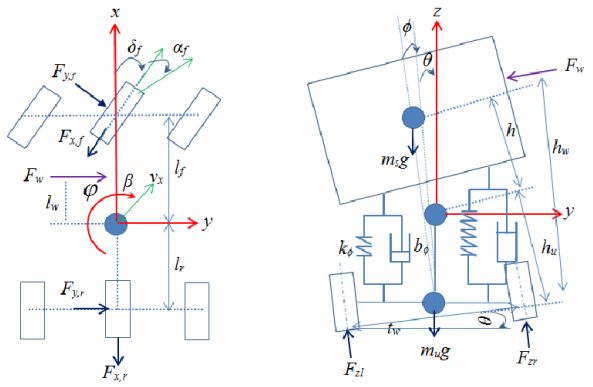

Fig. 1. Single truck model with roll DoF: (a) Top view; (b) front view.

2. Modeling and indicator

2.1 Double-track model

The vehicle model is described for the controller design, as shown in Fig. 1. We improved the vehicle model motions to account for the effects of wind and road bank angle. We made assumptions, such as $\sin\theta \approx 0$ and $\cos\theta \approx 1$, for small steering angles, roll angle and vehicle side slip angle. The front and rear suspensions are simplified by equivalent damping and stiffness coefficients. We considered the sprung vehicle mass and the suspension and wheel weights for un-sprung mass. Numerical data extracted from a single lorry are defined in Ref. [17].

In this paper, we use F_x, F_y and F_z to represent the longitudinal, lateral, and vertical tire forces, respectively. F_w represents the force exerted by side wind, while x, y and z are the coordinates of the car's position. t_w is the vehicle track width; ω_w is the angular velocity of the tires; v_x is the longitudinal wheel velocity; T_b is the wheel torque; α_f and α_r are the front and rear slip angles, respectively. δ_f and δ_r represent the steering angles of the front and rear wheels, respectively; μ acts as the track friction coefficient; θ is the road bank angle; ψ and φ are the heading angle and yaw rate, respectively; s is longitudinal tire slip ratio; β is the vehicle side slip angle; and ϕ and ς represent the roll and roll rate angle, respectively. The variables at the front and rear wheels are denoted by lower subscripts $(\cdot)_f$ and $(\cdot)_r$.

Using the assumption stated above for the motion longitudinal, lateral, yaw, roll, and rotational dynamics of the front and rear wheels of eight-Degrees of freedom (DoF) for the nonlinear model, vehicle motions containing the effect of disturbances are described in planar dynamics equations [18]:

$$\sum F_x : m(\ddot{x} - \dot{y}\varphi) = 2F_{xf} + 2F_{xr} - m_s h\dot{\varphi}\phi - 2m_s h\varphi\varsigma + (l_f - l_r)m_u \varphi^2 \quad (1)$$

$$\sum F_y : m(\ddot{y} + \dot{x}\varphi) = 2F_{yf} + 2F_{yr} + m_s h\dot{\varsigma} - m_s h\phi\varphi^2 - m_s h\phi\varsigma^2 + (l_r - l_f)m_u \dot{\varphi} + m_s g\theta + F_w \quad (2)$$

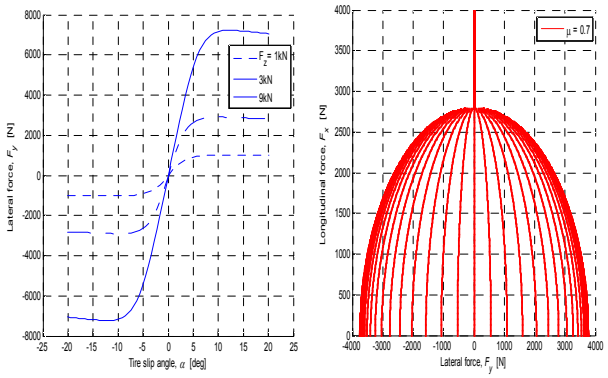

(a) (b)

Fig. 2. Semi-empirical tire model: (a) Lateral; (b) vertical forces.

$$\sum M_z : I_{zz}\ddot{\varphi} - I_{xz}\ddot{\varsigma} = {}^{t_w}\!/_{2}(-F_{xf,l}+F_{xf,r}-F_{xr,l}+F_{xr,r}) + 2l_fF_{yf} - 2l_rF_{yr} + (l_r - l_f)m_u(\ddot{y}+\dot{x}\dot{\varphi}) + M_{wz} \quad (3)$$

$$\sum M_x : (I_{xx}+m_sh^2)\ddot{\varsigma} + m_sh(\ddot{y}+\dot{x}\dot{\varphi}) - I_{xz}\ddot{\varphi} = m_s gh\phi - (k_{\phi f}+k_{\phi r})\phi - (b_{\phi f}+b_{\phi r})\dot{\varsigma} + M_{wx} + \dot{P}_b \quad (4)$$

$$J_b\dot{\omega}_{wi} = -r_wF_{xi} - T_{bi} - b_w\omega_i, \quad i=(f,r), \quad (5)$$

where M_{wz} and M_{wx} are the respective yaw moment and roll moment around the center of gravity of the vehicle when affected by wind. $P_b^{\cdot}$ in Eq. (4) represents the changing roll rate disturbance of the road bank, which can be obtained through the vehicle frame's fixed coordinates based on Euler angles [4]. If the pitch angle and pitch rate are small, $P_b^{\cdot}$ can be simplified as

$$\dot{P}_b \approx \ddot{\theta}. \quad (6)$$

The motion equations for the vehicle in an inertial frame or in a *Y-X* axis under an assumed small yaw angle are as follows:

$$\dot{X} \approx v_x - \dot{y}\psi, \qquad \dot{Y} \approx v_x\psi + \dot{y}. \quad (7)$$

2.2 Nonlinear tire model

We used a semi-empirical tire model called the Pacejka [19], in which the nonlinear characteristics of longitudinal and lateral forces on the front and rear tires are assumed to depend on the slip angle, longitudinal slip, normal force, and surface friction, as depicted in Fig. 2.

The nonlinear tire mentioned above should satisfy the following equation:

$$\sqrt{F_{xi}^2 + F_{yi}^2} \le \mu F_{zi}, \qquad i=(f,r). \quad (8)$$

The nonlinear kinematics related to the tire slip angles of the front and rear wheels, and the longitudinal tire slip ratio, are given such that

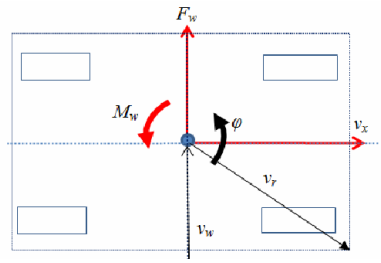

Fig. 3. Aerodynamic forces acting on the moving vehicle.

$$\alpha_f = \delta_f - \tan^{-1}\left(\frac{\dot{y}+l_f\psi}{\dot{x}}\right), \quad \alpha_r = \delta_r - \tan^{-1}\left(\frac{\dot{y}-l_r\psi}{\dot{x}}\right) \quad (9)$$

$$s = 1 - \frac{v_x}{r_w\omega_w}, \qquad \text{acceleration if } r_w\omega_w \ge v_x \quad (10)$$

$$s = \frac{r_w\omega_w}{v_x} - 1, \qquad \text{braking if } r_w\omega_w \le v_x. \quad (11)$$

2.3 Aerodynamic force and moment

When the vehicle is moving through strong wind, aerodynamic forces and moments are produced in all directions about the axles, as shown in Fig. 3. However, drag forces and pitch moment because of wind are ignored in this study. Wind force, yaw moment, and roll moment exerted by the wind are described by the following formula:

$$F_w = \frac{1}{2}C_y\rho S(v_x^2 + v_w^2) \quad (12)$$

$$M_{wz} = \frac{1}{2}l_wC_y\rho S(v_x^2+v_w^2), \quad M_{wx} = \frac{1}{2}h_wC_y\rho S(v_x^2+v_w^2) \quad (13)$$

where ρ is the density of air, v_w is the relative velocity of lateral wind, and S is the frontal area of the vehicle. The yaw moment coefficient C_y is a dimensionless parameter, and we use the results of C_y from a typical wind tunnel test [1]. The wind force and yaw moment coefficient are resolved with respect to the mass center of gravity of the vehicle. Next, we define the distance between the vehicle's aerodynamic center and center of gravity as l_w on the *X*-axis and h_w on the *Y*-axis, respectively, as shown in Fig. 1.

The wind attack angle β_w is given as the following function:

$$\beta_w = \arctan\left(\frac{v_w}{v_x}\right), \quad (14)$$

which is regarded as a constant value because the small variation attributed to the running state of the vehicle is disregarded.

2.4 Load transfer ratio

The Load transfer ratio (LTR) is the most reliable rollover indicator, regardless of vehicle configurations and operational conditions. More details on LTR can be found in Ref. [20].

For a two-axle heavy vehicle, LTR is defined as follows:

$$LTR = \frac{F_{zr} - F_{zl}}{F_{zr} + F_{zl}} \tag{15}$$

where F_{zl} and F_{zr} are defined as the vertical tire forces acting on the left and right sides of the wheels. LTR becomes 1 or -1 when Two wheels lift off (TWLO) the ground on one side of the vehicle. TWLO is equally dangerous to the occupants, and hence, LTR is not restricted by the bounds 1 and -1. A torque balance on the assumed horizontal roll axles in terms of suspension torques and vertical wheel force is given by

$$F_{zl}\frac{t_w}{2} - F_{zr}\frac{t_w}{2} + b_\phi \varsigma + k_\phi \phi = 0 . \tag{16}$$

The relationships among longitudinal force, longitudinal tire slip ratio, and normal load forces for front and rear wheels because of the load transfer caused by lateral accelerations are given by the following equations:

$$F_{zf} = \frac{l_r mg}{2l} - \frac{F_{yf}\phi}{2} - \frac{k_{\phi f}\phi}{t_w} - \frac{b_{\phi f}\varsigma}{t_w} - \frac{h_{uf}F_{yf}}{t_w} - \frac{h_{uf}l_r mg\phi}{t_w l} \tag{17}$$

$$F_{zr} = \frac{l_f mg}{2l} - \frac{F_{yr}\phi}{2} - \frac{k_{\phi r}\phi}{t_w} - \frac{b_{\phi r}\varsigma}{t_w} - \frac{h_{ur}F_{yr}}{t_w} - \frac{h_{ur}l_f mg\phi}{t_w l} . \tag{18}$$

If we consider the un-sprung mass and lateral acceleration in the vertical forces in Eqs. (17) and (18) for the LTR in Eq. (15), then the function in Eq. (16) can be transformed to

$$LTR = \frac{\frac{2}{t_w}\left[b_\phi \varsigma + k_\phi \phi + h_{uf} m_s (\dot{v}_y + v_x \varphi - h\dot{\varsigma}) + h_{uf}(\frac{l_r mg}{l})(\phi + \theta) \right]}{mg} . \tag{19}$$

3. Disturbance estimation and control allocation

3.1 Controller model

In this sub-section, we design the controllers based on linearizing vehicle and tire models explained in Sec. 2, assuming constant forward speed. The controllers are designed based on 3-DoF lateral-roll motions without disturbance parameters, because we assume the disturbances are unmeasured:

$$m\dot{v}_y = \frac{1}{I_{xx}v_x}[-(C_r + C_f)J_{xq}v_y + ((C_r l_r - C_f l_f)J_{xq} - I_{xx}mv_x^2)\varphi] - \frac{1}{I_{xx}}[m(hb_\phi)\varsigma - mh(mgh - k_\phi)\phi - C_f J_{xq}\delta_f] \tag{20}$$

$$I_{zz}\dot{\varphi} = \frac{1}{v_x}[(C_r l_r - C_f l_f)v_y - (C_f l_f^2 + C_r l_r^2)\varphi] + C_f l_f \delta_f \tag{21}$$

$$I_{xx}\dot{\varsigma} = \frac{h}{v_x}[(C_r l_r - C_f l_f)\varphi - (C_f + C_r)v_y] - b_\phi \varsigma + (mgh - k_\phi)\phi + C_f h\,\delta_f , \tag{22}$$

where J_{xq} in Eq. (20) is the roll moment of the vehicle about the roll axle.

The vehicle model in Eqs. (20)-(22) with disturbances can be transferred to a state-space function as follows:

$$\dot{x} = Ax + B_1 u + B_d w_d , \quad y = Cx + Du . \tag{23}$$

$A \in \mathbb{R}^{6x6}$ is the known state matrix, $B_1 \in \mathbb{R}^{6x1}$ is the input matrix, $C \in \mathbb{R}^{1x6}$ is the output matrix, and $B_d \in \mathbb{R}^{6x3}$ is the disturbance input matrix. We define them as

$$x = [v_y\ Y\ \varphi\ \psi\ \varsigma\ \phi]^T,\ u = [\delta_f],\ w_d = [F_w\ \theta\ \dot{P}_b]^T,\ y = [LTR] . \tag{24}$$

3.2 DOB design

We estimate the wind pressure on the vehicle and road bank using the state-space disturbance observer method. The disturbance input w_d is a linear waveform description interpreted as

$$\dot{x}_w = A_w x_w , \quad w_d = C_w x_w , \tag{25}$$

where $x_w \in \mathbb{R}^{xw}$ is the disturbance states vector and $w_d \in \mathbb{R}^{wd}$ is the disturbance vector. w_d is one of the state variables, which is estimated by the following equation, and combined with Eqs. (23) and (25):

$$\begin{bmatrix} \dot{x} \\ \dot{x}_w \end{bmatrix} = \begin{bmatrix} A & B_d \\ 0 & A_w \end{bmatrix}\begin{bmatrix} x \\ x_w \end{bmatrix} + \begin{bmatrix} B_1 \\ 0 \end{bmatrix} u \tag{26}$$

$$Y = \begin{bmatrix} C & 0 \end{bmatrix}\begin{bmatrix} x \\ x_w \end{bmatrix} . \tag{27}$$

Using the model developed in Eqs. (26) and (27), we obtain the estimated state $\hat{x}$ and estimated disturbance input $\hat{w}_d$. An augmenting equation is given by

$$\begin{bmatrix} \dot{\hat{x}} \\ \dot{\hat{x}}_w \end{bmatrix} = \begin{bmatrix} A & B_d \\ 0 & A_w \end{bmatrix}\begin{bmatrix} \hat{x} \\ \hat{x}_w \end{bmatrix} + \begin{bmatrix} B_1 \\ 0 \end{bmatrix} u + M(\dot{\hat{Y}} - \hat{Y}) \tag{28}$$

$$\hat{Y} = \begin{bmatrix} C & 0 \end{bmatrix}\begin{bmatrix} \hat{x} \\ \hat{x}_w \end{bmatrix} . \tag{29}$$

We can express the error $e = \hat{x} - x$ with respect to the parameters of the system from the differential of Eqs. (26) and (28), which yields:

$$\dot{e}(t) = (A + MC)e(t) . \tag{30}$$

Eq. (30) is called an asymptotic state observer. The observer gain M is designed by the pole assignment. We can ensure that error converges towards zero, while setting all eigenvalues of $A + MC$ with a negative real part with respect to M.

Because LTR cannot be estimated directly in real time, an indirect estimate method depending on the roll motion is proposed. Roll rate can be estimated directly using a GPS altitude system combined with an automotive grade gyroscope oriented to measure roll rate. Consequently, the roll angle is calculated from the measured roll rate. Yaw rate can be measured by a gyroscope or a virtual sensor, or synthesized from accelerometers. GPS measurements contain high levels of noise compared to traditional inertial sensors, and hence, white noise is added to the measured state. The noise also has a significant effect on the estimated disturbance input as the main reason for the disturbance estimation error.

3.3 LQC design

A disturbance observer is applied to provide steering assistance to the driver, as shown in Fig. 4. $\varepsilon(t)$ is the control error, $\tilde{w}(t)$ is the state error of the integral compensator, and $\tilde{u}(t)$ is the input error, and are defined as follows:

$$\varepsilon(t)=r(t)-y(t)=\dot{w}(t),\ \tilde{w}(t)=w(t)-w_{\infty},\ \tilde{u}(t)=u(t)-v_{\infty}, \quad (31)$$

where w_{∞} and u_{∞} are defined as the steady-state value when the offset becomes zero. The cost function, including the state error of the integral compensator, is used to generate the LQC gain matrix:

$$J_{lqc}=\int_0^{\infty}(\varepsilon^T(t)Q_{lq1}\varepsilon(t)+\tilde{w}^T(t)Q_{lq2}\tilde{w}(t)+\tilde{u}^T(t)R_{lq}\tilde{u}(t))dt, \quad (32)$$

where, Q_{lq1}, Q_{lq2} and R_{lq} are all positive-definite weighting matrices. The terms $\varepsilon^T Q_{lq1}\varepsilon$ and $\tilde{w}^T Q_{lq2}\tilde{w}$ are used to solve state regulation problems. The term $\tilde{u}^T R_{lq}\tilde{u}$ is used to minimize the energy $u(t)$ where the control input is bounded such that $u_{min} \le u(t) \le u_{max}$.

We attempt to determine the control input $u(t)$ that will regulate the system at zero by tuning Q_{lq1}, Q_{lq2} and R_{lq}. The optimal input state feedback controller K_{opt} is obtained by minimizing the cost function:

$$K_{opt}=[-R_{lq}^{-1}B_1^T P_{11} \quad -R_{lq}^{-1}B_1^T P_{12}], \quad (33)$$

where P_{11} and P_{12} are the unique positive-definite solutions to the Riccati differential equation [21].

Here, the feedforward gain K_s, which is designed for target tracking, and the feedback gain K_f, are described as follows:

$$K_s=[-C(A+B_1K_{opt})^{-1}B_1]^{-1},\ K_f=C(A+B_1K_{opt})^{-1}. \quad (34)$$

The control law with an integral compensation can be derived as follows:

$$z(t)=w(t)+K_f\hat{x}=-K_p x-(K_e-K_f)\hat{x}=K_p(\hat{x}-x) \quad (35)$$

where

$$K_p=(I+K_fM)C(A+MC)^{-1},\quad K_e=K_f-K_p, \quad (36)$$

where $\hat{x}\approx x$, $z(t)$ is approximately zero. Next, while the initial value is set to zero, the integral-type controller can be derived as follows:

$$u(t)=K_{opt}\hat{x}+Gz(t)+K_s r(t)=(K_{opt}+GK_p)\hat{x}-Gx+K_s r(t). \quad (37)$$

Finally, the front steering angle with compensation for disturbance rejection can be described as

$$\delta_f(t)=u(t)-M_w(s)\hat{F}_w-M_b(s)\hat{\theta}-M_p(s)\hat{\dot{P}}_b, \quad (38)$$

where $M_w(s)$, $M_b(s)$ and $M_p(s)$ represent the Low-pass filters (LPF), which will be introduced in Sec. 3.5.

3.4 MPC design

The block diagram of the MPC is illustrated in Fig. 4. Because MPC is designed in discrete-time, we discretize the vehicle dynamics in Eq. (23) without unmeasured disturbances to obtain

$$x(k+1)=Ax(k)+B_1u(k),\quad y(k)=Cx(k)+Du(k), \quad (39)$$

where $x(k)$ is the state vector at time step k and $x(k+1)$ is the state vector at time step $k+1$. $u(k)$ is defined as the optimal input calculated by the MPC optimizer. The front steer angle $\delta_f(k)$ with compensation for disturbance rejection can be described as

$$\delta_f(k)=u(k)-O_w(s)\hat{F}_w-O_b(s)\hat{\theta}-O_p(s)\hat{\dot{P}}_b. \quad (40)$$

The aim of the MPC optimizer is to obtain the optimal control input vector $\Delta\bar{u}(k+i)$, to ensure that the error between the predicted output $\bar{y}(k+i)$ and the reference signal $r(k+i)$ can be minimized. The optimization of the predictive control system is achieved by minimizing the cost function:

$$\begin{aligned} Minimize: J_{mpc}(k)=&\sum_{i=1}^{H_p}\left\|\bar{y}(k+i)-r(k+i)\right\|^2_{S_q(i)}\\ &+\sum_{i=0}^{H_c-1}\left\|\Delta\bar{u}(k+i)\right\|^2_{S_r(i)} \end{aligned}. \quad (41)$$

The weight matrices $S_q(i)$ and $S_r(i)$ are diagonal matrices that can be adjusted for the desired closed-loop performance. The variation of the front steer angle $\Delta\bar{u}(k+i)$ can be obtained when the cost function is as small as possible. The prediction and control horizon are described as H_p and H_c, and is

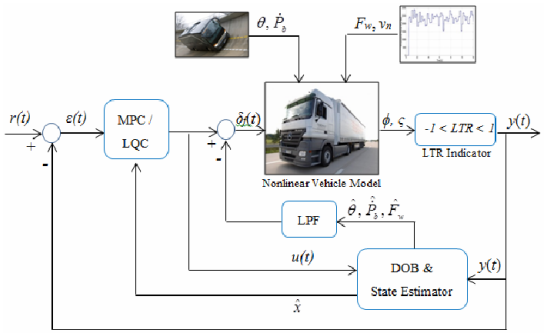

Fig. 4. Block diagram of MPC and LQC with DOB for truck vehicle.

assumed $H_p \geq H_c$. We formulate the optimization of the predictive control system while taking the constraints of steering actuators into consideration, such as the operating range of the front tires. At every time step, the controller solves an optimization problem that can be written as

$$\begin{aligned} &\min : J_{mpc}(x(k), \Delta u(k)) \\ &subject\ \ to: \\ &\qquad \bar{x}(k+1) = Ax(k) + B_1 u(k) \\ &\bar{x}(k+2) = A\bar{x}(k+1) + B_1 \bar{u}(k+1) \\ &\qquad \vdots \\ &\qquad \bar{x}(k+i) = A\bar{x}(k+i-1) + B_1 \bar{u}(k+i-1) \\ &\qquad \left|\bar{u}(k+i)\right| \leq \delta_f \\ &\qquad \left|\Delta\bar{u}(k+i)\right| \leq \Delta\delta_f \\ &\left|\bar{y}(k+i)\right| \leq LTR \quad (i = 1, \cdots H_p) \end{aligned} \tag{42}$$

In the MPC concept, only the first input sample of the complete optimal sequence is applied to the process. New samples are taken to determine the current state of the system, and the entire procedure is repeated.

3.5 Low-pass filter and white noise

An LPF called Q-filter [22] is utilized in the feedback signals of DOB to limit compensation to a preselected low frequency range. Filter $M_i(s)$ is designed for LQC, while filter $O_i(s)$ is added in MPC. The transfer functions of the two filters are expressed as follows:

$$M_i(s) = \frac{F_i}{\eta_i s + 1}, \qquad O_i(s) = \frac{G_i}{\xi_i s + 1}, \tag{43}$$

where η_i and ξ_i are the filter time constants, F_i and G_i are the filter pass-band gain, while subscript i is nominated to be w, b and p, to constitute three cancellation signals. The cut-off frequency of the filter is the reciprocal of its filter time constant. The cut-off frequency for wind is 50 Hz and 100 Hz for the road bank, while considering the unstructured external disturbances and observation noise. The tuning of F_i and G_i for each filter is conducted through trial and error.

The LPF plays a significant role in determining the robustness and disturbance suppression performance of the system. For a disturbance signal in which maximum frequency is lower than the cut-off frequency of the LPF, the disturbance signal is considered to be effectively rejected, and the real plant behaves as a nominal plant.

Note that white noise v_n is added to the observed roll rate and roll angle. The mean and power spectral density of white noise is set to [0.1, 3.5 × 10^{-5}].

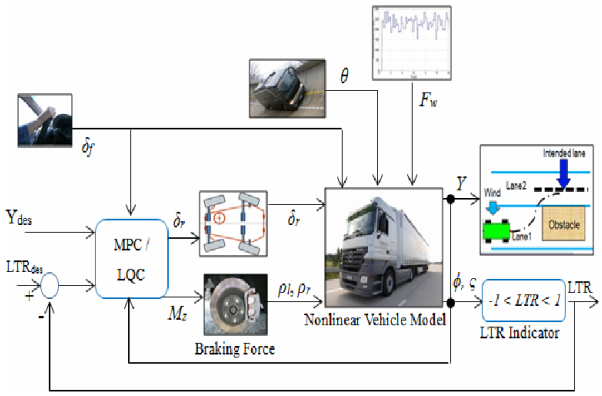

Fig. 5. Vehicle control via ARS and DBC maneuver control.

3.6 MPC design for ARS with DYC

This section presents the second contribution of this paper. The block diagram of the controller design of MPC is illustrated in Fig. 5. The MPC is designed to track the lane in a single lane change maneuver using ARS and DBC and prevents rollover. The MPC is designed as in Eqs. (20)-(22), with additional rear steering and braking control as a control input to the system.

We discretize the vehicle dynamics to obtain

$$x_{2l}(k+1) = A_2 x_{2l}(k) + B_2 u_{2l}(k) + B_{2d} w_{2dl}(k) \tag{44}$$

$$y_{2l}(k) = C_2 x_{2l}(k) + D_2 u_{2l}(k)\,. \tag{45}$$

The state vectors, control signals, and desired outputs are represented by

$$\begin{aligned} &x_{2l}(k) = [v_y\ Y\ \varphi\ \psi\ \varsigma\ \phi\ \omega_{f,r}\ \omega_{f,l}\ \omega_{r,r}\ \omega_{r,r}]^T,\ u_{2l}(k) = [\delta_r\ \rho_r\ \rho_l]^T \\ &w_{2dl}(k) = [\delta_f],\quad y_{2l}(k) = [Y\ \ LTR]^T\,. \end{aligned} \tag{46}$$

We use braking force ρ to realize rollover prevention by considering the differential braking force acting on either the left or right side of the wheel as follows:

$$\rho_i = \frac{t_w}{2J_{zz}}\,. \tag{47}$$

We define the braking force exerted on the left side as the forward direction, while an anticlockwise yaw moment M_z is yielded as shown in Fig. 6.

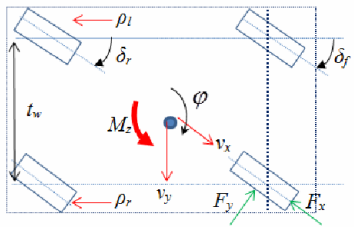

Fig. 6. Differential braking control.

4. Simulation

4.1 Scenario description

In the first scenario, we mitigate roll motion while running the heavy vehicle without a driver under strong winds and road bank disturbance. We assume that the vehicle is moving in a straight path over wide open ground at a speed of v_x = 55 km/h. The autonomous steering control is simulated in two different environmental conditions: (i) Step wind of a typhoon, and (ii) combination of sinusoidal wind of a typhoon with a random road bank angle.

It is important to highlight that the weighting matrices for the input and outputs of MPC and LQC are selected from the best output responses of repetitive implementation, concentrating on the output weighting gain rather than on the input weighting gain. Furthermore, the reference value is set to zero, which means the LTR and roll angle are in turn mitigated to zero.

In the second scenario, the controllers of the proposed methods, mentioned in Sec. 3.6, are implemented in a simulated thread avoidance scenario. The vehicle is considered to be travelling at a constant speed (55 km/h), without braking or accelerating. The typical obstacle avoidance maneuver is simulated with a peak driver steering input magnitude of 10 deg at t = 2 s acting as disturbance on the vehicle. All simulation scenarios were performed using the Model predictive control toolbox in Matlab and Simulink software within 15 s.

4.2 Autonomous control under wind step

Vehicle behavior is strongly affected by wind in real life. We refer to the typhoon level as defined by the Japan Meteorological Agency. Here, the step wind speed considered a strong typhoon is set to v_w = 220 km/h, while the attack angle is β_w = 75.96 deg.

We set the eigenvalues of $A + MC$ far from reality to obtain better convergence to the estimated wind force. The eigenvalues for the DOB design and weighting matrices of the MPC and LQC are described in Tables 1 and 2. For the LQC design, the cut-off frequency and filter pass-band gain are set at 50 Hz and 1.5, respectively, and we can obtain

$$M_w(s) = \frac{1.5}{0.02s+1}, \quad M_b(s) = M_p(s) = 0 . \tag{48}$$

For the MPC design, LPF O_i is

Table 1. Disturbance observer design parameters.

Parameter	Value
Eigenvalues of ($A + MC$) of observer	-18 + 6j
	-18 - 6j
	-15 + 5j
	-15 - 5j
	-13 - 4j

Table 2. MPC and LQC controller parameters.

Parameter	MPC	LQC
H_p, H_c	20, 9	20
T_s [s]	0.05	0.05
δ_f [deg]	± 20	± 20
LTR	± 1	± 1
S_r, R_{lq}	0.1	2
S_{q1}, S_{q2}, Q_{lq1}, Q_{lq2}	4.5, 2.5	10, 5

$$O_w(s) = \frac{1.1}{0.02s+1}, \quad O_b(s) = O_p(s) = 0 . \tag{49}$$

Fig. 7 shows the simulated results of the estimated wind force using the proposed disturbance observer. The estimation fluctuates with the effect of white noise, which is discussed in Sec. 3.5. The estimated wind force is verified with its real value from the estimation error. The wind estimation is within the accuracy of the wind measurement and rollover prevention system, suggesting that dynamic separation works well.

Fig. 7 shows that the LTR response without control exceeds the average of 1.25 by 1, indicating that the left side of the tires loses contact with the ground because of the effects of the strong winds acting on the left side of the vehicle body. This condition indicates that the vehicle is at risk of fatal rollover accidents. Although steady-state error in both controllers is kept at zero, the settling time with the MPC controller is faster than that of LQC. The overshoot with the MPC controller also mitigates more, compared to LQC. Furthermore, the undershoot in LQC is revised by DRC based on DOB.

The front steer angle $\delta_f(k)$ using MPC is generated slightly faster than using LQC after 2 s, mainly because of the predicted effect of MPC, as shown in Fig. 7. The predicted effect of MPC is also the reason for less overshoot of the disturbance response. However, in the MPC control system, the controlled $\delta_f(k)$ makes small reciprocating vibrations because of the precise control following the estimated disturbance. In the following simulations, improvements for negating the perturbations of front steering are discussed.

4.3 Autonomous control on a bumpy road with sinusoidal wind

Vehicle movement on a bumpy road through strong winds is the worst possible condition. Roll motion is unexpected because of the effects of random disturbances combined with

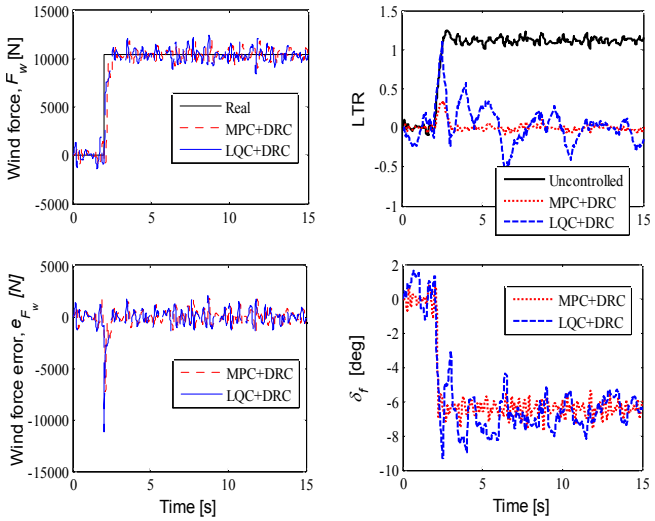

Fig. 7. Autonomous control under the step wind.

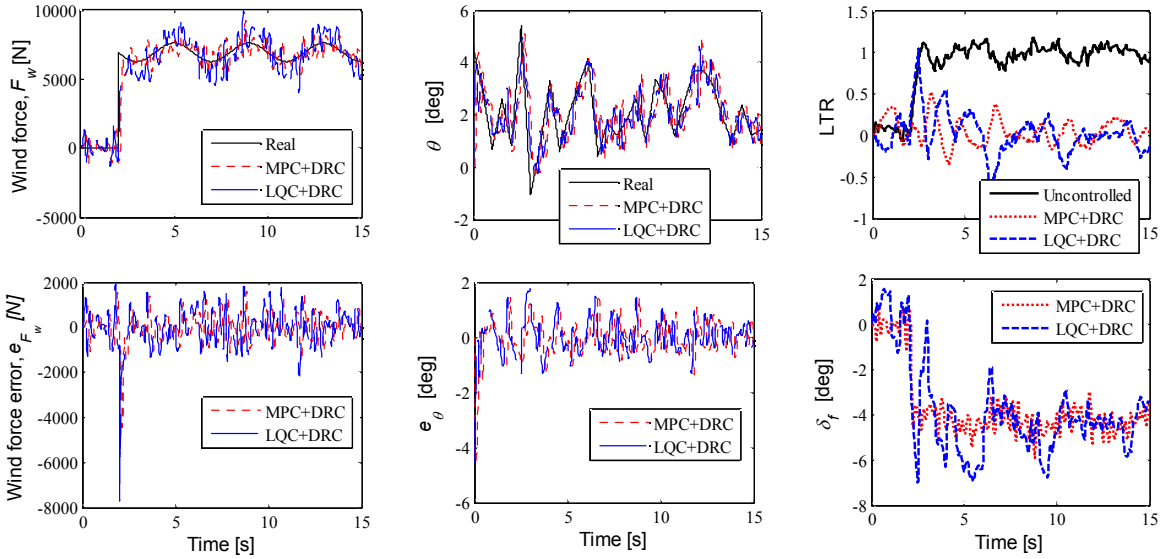

Fig. 8. Autonomous control on the bumpy road under the sinusoidal wind.

random road banks and sinusoidal winds.

Real bank angle is simulated as "Gaussian noise", of which the variance, mean, and frequency are 2, 2 and 2, respectively. Here, the bank angle is estimated using DOB. Our aim is to assess vehicle behavior and suppress the vibration around the roll motion in the sine-wave disturbance response. The average speed of the wind sine-wave is considered a small typhoon, set at v_w = 165 km/h, and its frequency is set at 0.25 Hz. The attack angle is β_w = 71.56 deg. The wind disturbance is set as the sine-wave strong wind described in Fig. 8.

LPF design in each control system is given by

$$M_w(s) = \frac{1.2}{0.02s+1}, \quad M_b(s) = M_p(s) = \frac{1.1}{0.01s+1} \tag{50}$$

$$O_w(s) = \frac{1.1}{0.02s+1}, \quad O_b(s) = O_p(s) = \frac{1}{0.01s+1}. \tag{51}$$

The road bank angle estimation can be found in Fig. 8, and may be used to find $P_b^{\cdot}$. Similar to the results of wind force estimation, the road bank angle was successfully estimated.

In Fig. 8, the LTR of the uncontrolled case increases significantly under the effects of sinusoidal wind and road bank, compared to the results of previous simulations, which only considered step wind, as seen in Fig. 7. The abrupt increase and variation of LTR is generated when the positive values of two disturbances are combined. A positive value of both disturbances combined around their peach value enables LTR to exceed the limit.

Overall, the LTR controlled by LQC exhibited inferior vibration suppression, and its oscillation was larger, starting at 2 s, compared to the LTR controlled by MPC. The MPC controller demonstrated good vibration suppression throughout the response. The LTR response from MPC with DRC was almost 30% less than in LQC with DRC on average. Furthermore, with the compensation of the DRC, the disturbance from high frequency was cancelled more effectively in both controllers.

Fig. 8 shows the results of the front steer angle δ_f from each of the controllers, where δ_f in all cases is limited to ± 10 degrees. In spite of the similar behaviors of δ_f in both controllers, the MPC controller with DRC assists steering to achieve accurate tracking control. Simulations have shown that the DOB-MPC advanced control can achieve far superior disturbance rejection performance than the DOB-LQC. Moreover, disturbance rejection and set-point tracking performance can be regulated separately by tuning the corresponding adjustable parameters in DOB and MPC, which is convenient for practical engineering applications.

Table 3. Controller parameters condition in ARS+DBC maneuver.

Parameter	MPC	LQC
H_p, H_c	20, 9	9
T_s [s]	0.05	0.05
δ_r [deg], $\Delta\delta_r$ [deg/s]	±30, ±20	±30, ±20
ρ [Nm], $\Delta\rho$ [Nm/s]	±1500, ±1000	±1500, ±1000
S_{r1}, S_{r2}	0.1, 0.1	5, 5
S_{q11}, S_{q22}	0.00221, 0.00951	0.00521, 0.01505

4.4 ARS with DBC under disturbance of front wheel steering

In this sub-section, we study DBC by utilizing the rear braking forces between the left and right sides of the rear tires. The normal step wind speed is set at v_w = 36 km/h, with a bank angle θ = 10 deg. We compared the performance of the controller design for thread avoidance and rollover prevention through ARS with the DBC maneuver control. We set the single lane change maneuver at a 10 deg step input, representing the distance from the initial condition (0 meters) to 10 meters, starting from t = 0.5 s or Y_{ref} = 10 deg. Table 3 lists the controller parameters in ARS with the DBC maneuver.

We investigate the effectiveness of the proposed braking control allocation, as described in Sec. 3.6, under the disturbances. Fig. 9 shows the responses of the vehicle's motion through ARS with the DBC maneuver control of the MPC and LQC. Without the controller, the single lane change maneuver clearly fails to follow the trajectory, resulting in a high probability of collision. The response of the LTR motion indicates that the vehicle is not stable when one side of the tire is not in contact with the ground and the trajectory is ongoing. However, no rollover occurs because it is less than 1. Moreover, we can scrutinize the lateral acceleration of unstable vehicles when it shows acceleration is infinite after 5 s.

Fig. 9 shows the vehicle responses performed well with the controller, either to the MPC or the LQC. Both controllers

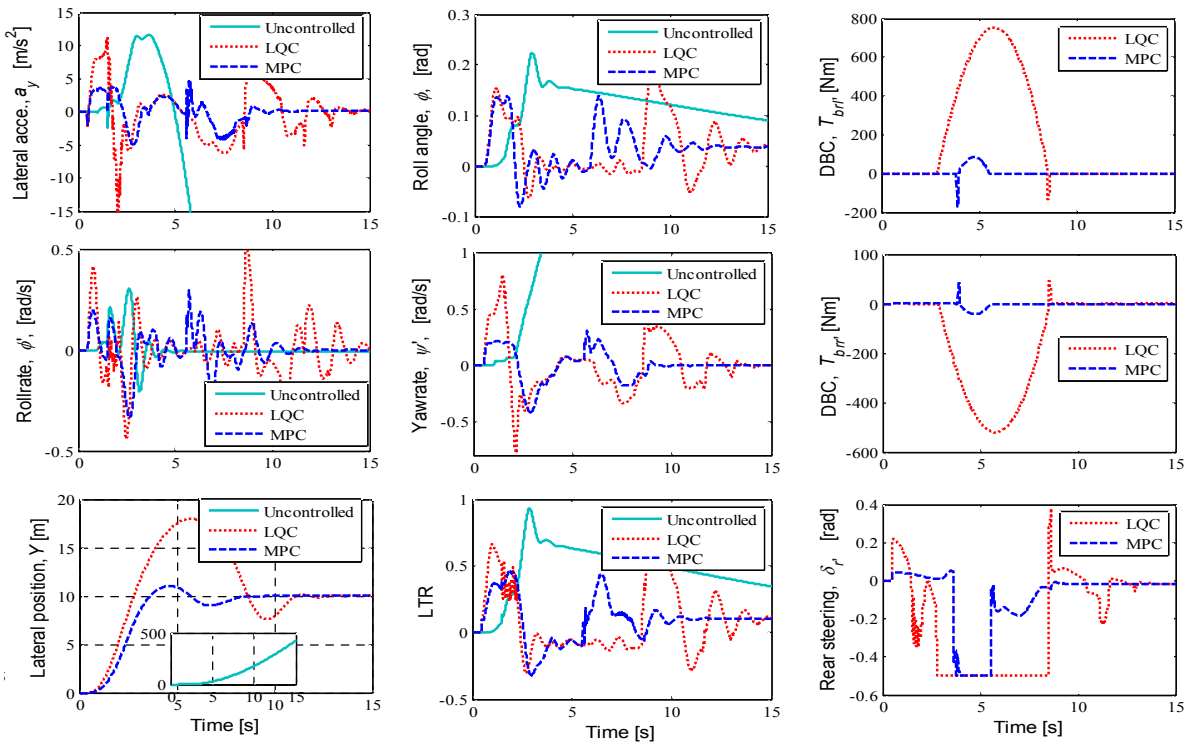

Fig. 9. Vehicle is performed at v_x = 55 km/h under disturbances with controller.

performed well for the LTR response, meaning both sides of the wheels touch the ground, and no rollover occurred during the maneuver under disturbance. Both controllers also performed very well, and yaw rate response was less than ±0.5 deg/s indicating vehicle yaw stability.

Moreover, the lateral and LTR responses illustrate that MPC is more effective and successful than LQC at achieving the desired path, further indicating that DBC affects the control lane maneuver change at the reference. The figure also demonstrates that the lateral acceleration for both controllers is stable when the steady state of acceleration is zero. Furthermore, the control signal responses show that both controllers were constrained under rear steering input command, during which DBC takes over control of the vehicle by applying brake torque between the left and right rear wheels. The ARS and DBC maneuvers indicate the advantages of the MPC approach when implemented in multivariable and constrained systems.

5. Conclusions

The rollover prevention control in the worst-case environments was presented and evaluated by driving a vehicle along a straight path without human intervention. The proposed disturbance observer and measurements for lateral wind and road bank were applied to estimate the wind force and road bank angle separately.

The MPC and the LQC both satisfied the requirements for the reference of LTR tracking and suppression. However, MPC exhibited showed better cancellation of constant sinusoidal or random disturbance than LQC. Some points are highlighted as follows:

MPC led to better and faster optimal operation of front steering than LQC, and could reduce LTR based on prediction time. In this study, the front steering controlled by MPC moved approximately 0.5 s in advance without additional filtering.

MPC was proven to better compensate for sinusoidal and random disturbances.

The DOB-based DRC was executed by the MPC and the LQC controller to decrease the effects of wind and road bank. The LPF was successfully adopted to achieve the desired fading action. Currently, we are seeking to solve the trade-off between rollover prevention and trajectory tracking in inclement environments.

An integrated control approach for an ARS and DBC maneuver of heavy vehicles in a thread avoidance scenario in an inclement environment was also presented. ARS controlled the rear steering, while DBC controlled the differential rear braking between the left and right wheels. The simulation results demonstrated that MPC control performance was better than LQC in terms of the LTR and *Y*-displacement.

The improvement of the control method using different combinations, such as active rear steering, active suspension, and braking with front and rear wheels, may be investigated further in future work. The proposed method is suggested for implementation in real world applications.

Acknowledgment

This work is supported by the Tokyo Metropolitan Government Japan under Asian Human Resources Fund.

References

[1] S. Glaser, S. Mammar and D. Dakhlallah, Lateral wind force and torque estimation for a driving assistance, *17th World Congress*, Seoul, Korea, 17 (1) (2008) 5688-5693.

[2] B. A. Güvenç, L. Güvenç and S. Karaman, Robust MIMO disturbance observer analysis and design with application to active car steering, *Int. J. Robust Nonlinear Control*, 20 (8) (2010) 873-891.

[3] H. Kitano, O. Nishihara, M. Kurishige and T. Matsunaga, Estimation of lateral disturbance with observer and compensation control with electric power steering, *Trans. Jpn. Soc. Mech. Eng. Ser. C*, 78 (795) (2012) 3715-3729.

[4] J. Ryu and J. C. Gerdes, Estimation of vehicle roll and road bank angle, *Am. Control Conf.*, Boston, MA, USA (2004) 2110-2115.

[5] Y. Sebsadji, S. Glaser, S. Mammar and M. Netto, Vehicle roll and road rank angles estimation, *17th World Congress*, Seoul, Korea, 17 (1) (2008) 7091-7097.

[6] G. Yu, D. Wang, Q. Li, P. Wang and Y. Wang, Road bank estimation for bus rollover prediction, *Appl. Math. Inf. Sci*., 7 (5) (2013) 2027-2034.

[7] D. Edouard, P. Dufour and H. Hammouri, Observer based multivariable control of a catalytic reverse flow reactor: comparison between LQR and MPC approaches, *Comput. Chem. Eng*., 29 (4) (2005) 851-865.

[8] S. Franko, I. M. Koc, C. Ozsoy and N. Sari, MPC and LQR type controller design and comparison for an unmanned helicopter, *Proc. 2011 Sum. Comput. Simul.,* Hague, Netherlands (2011) 138-144.

[9] D. Meola, G. Gambino, G. Palmieri and L. Glielmo, A comparison between LTV-MPC and LQR yaw rate-side slip controller engine and powertrain control, simulation and modeling, *Proc. of IFAC Workshop on Eng., and Powertrain Control, Sim., and Mod*., France (2009) 154-159.

[10] Q. Zou, Optimal preview-based stable inversion for output tracking of nonminimum-phase systems, *Automatica*, 45 (1) (2009) 230-237.

[11] Y. D. Yoon, E. Jung and S. K. Sul, Application of a disturbance observer for relative position control system, *IEEE Trans. Ind. Appl*., 46 (2) (2010) 849-856.

[12] J. Yang, S. H. Li, X. S. Chen and Q. Li, Disturbance rejection of dead-time processes using disturbance observer and model predictive control, *Chem. Eng. Res. Des.*, 89 (2) (2011) 125-135.

[13] K. M. Junaid and S. Wang, Autonomous vehicle follow-

ing performance comparison and proposition of a quasi-linear controller, *J. Info. Tech. and Control*, 36 (4) (2007) 393-401.

[14] F. Yakub and Y. Mori, Comparative study of autonomous path-following vehicle control via model predictive control and linear quadratic control, *J. of Automobile Eng., Part D* (2015) doi: 10.1177/0954407014566031.

[15] J. Tjonnas and T. A. Johansen, Stabilization of automotive vehicles using active steering and adaptive brake control allocation, *IEEE Trans. on Control Systems Technol.*, 18 (3) (2010) 545-558.

[16] A. Ghaffari, S. H. T. Oreh, R. Kazemi and M. A. R. Karbalaei, An intelligent approach to the lateral forces usage in controlling the vehicle yaw rate, *Asian J. of Control*, 13 (2) (2011) 213-231.

[17] L. Shihao, F. Yakub, M. Kasahara and Y. Mori, Rollover prevention with predictive control of differential braking and rear wheel steering, *Proc. of 6th Int. Conf. Rob., Auto. and Mecha.*, Manila, Philippines (2013) 144-149.

[18] F. Yakub and Y. Mori, Heavy vehicle stability and rollover prevention through switching model predictive control, *Asian Control Conf.*, Kota Kinabalu, Malaysia (2015) 1-6.

[19] H. B. Pacejka, *Tire and Vehicle Dynamics*, Third Ed., Elsevier Ltd, Oxford (2012).

[20] S. Solmaz, M. Corless and R. Shorten, A methodology for the design of robust rollover prevention controllers for automotive vehicles: Part 2-Active steering, *Am. Control Conf.*, New York, USA (2007) 1606-1611.

[21] K. P. Groves, D. O. Sigthorsson, A. Serrani, S. Yurkovich, M. A. Bolender and D. B. Doman, Reference command tracking for a linearized model of an air-breathing hypersonic vehicle, *Proc. of AIAA Guidance, Navigation, and Control Conf.*, California, USA (2005) 1-14.

[22] B. A. Guvenc, T. Bunte, D. Odenthal and L. Guvenc, Robust two degree-of-freedom vehicle steering controller design, *IEEE Control Syst. Technol.*, 12 (4) (2004) 627-636.

Fitri Yakub received his Dip.E., and B.E. degrees in Mechatronics and Electronics Eng. from the University of Technology Malaysia in 2001 and 2006, respectively. He obtained his M.Sc. in Mechatronics Eng. from the International Islamic University Malaysia in 2011. He received his Ph.D. degree in Mechatronics Eng. from Tokyo Metropolitan University under Asian Human Resource Fund by Tokyo Metropolitan Government from 2012 to 2015. He is currently with the Malaysia-Japan International Institute of Technology. He is a senior member of IEEE, and is a member of SAE, SICE and IET.

Lee Shihao received his B.S. degree in Mechanical Engineering from Shanghai University of Engineering Science in 2009. He obtained M.Sc. in Mechatronics Engineering from Tokyo Metropolitan University in 2014, where he focused on active motion control system. He is currently working with Hitachi Ltd, Ibaraki, Japan.

Yasuchika Mori received his B.S., M.S. and Ph.D. degrees in Electrical Engineering from Waseda University, Japan in 1976, 1978 and 1981, respectively. From 1981 to 1987, he worked at the R&D Center of Toshiba Corporation, Japan. He is currently the Dean of Graduate School of System Design, Tokyo Metropolitan University, Japan. He is a member of IEEE, IFAC, ISCIE, senior member of IEEJ and fellow of SICE. His field of research interest includes digital control and design, automatic and robust control, stochastic control and RFID.